Supporting Information

Herman et al. 10.1073/pnas.1307154110

SI Materials and Methods

Animal Preparations. All procedures were performed in accordance with protocols approved by the Yale Institutional Animal Care and Use Committee (IACUC) and in agreement with the National Institutes of Health guide for the care and use of laboratory animals. Isoflurane (1–2%) anesthetized Sprague–Dawley rats were tracheotomized and artificially ventilated (70% N_2O, 30% O_2). The anesthesia was switched to α-chloralose (80-mg initial dose then 40 mg·kg^{-1}·h^{-1}, intraperitoneal) after the surgical phase. A femoral arterial line was used for monitoring blood pressure, acid–base balance and blood gases throughout the experiment. A femoral i.v. line was used for administration of additional volumes (saline and sodium bicarbonate), tubocurarine chloride (0.3 mg·kg^{-1}·h^{-1}), and functional MRI (fMRI) contrast agents as needed. The core temperature was maintained at 37 °C with a heated water blanket. Physiological variables (pCO2, pO2, pH, and blood pressure) were measured and kept within normal limits (37 ± 3 mm Hg, 102 ± 15 mm Hg, 7.36 ± 0.03, and 108 ± 12 mm Hg, respectively). Thin copper wires were inserted below the skin between carpal and metacarpal pads for functional stimulation of the forepaw by electrical pulses (0.3 ms, 3 Hz, 2 mA) for 30-s duration, with a 5-min delay in between stimulations. The recording session began after a 1.5-h waiting period, while the anesthesia stabilized.

Neurophysiological Experiments. Rats (n = 32) were placed in a stereotaxic holder on a vibration-free table inside a Faraday cage. Tiny burr holes above the forepaw (i.e., S1FL) somatosensory regions (4.4 mm lateral and 1.0 mm anterior to Bregma) were drilled and high-impedance tungsten microelectrodes (FHC Inc.) together with micro laser Doppler probes (Oxford Optronics) were inserted gradually into the cortex (upper layers, 0.30 ± 0.05 mm; middle layers, 0.90 ± 0.05 mm; and lower layers, 1.50 ± 0.05 mm) after waiting for the stabilization period. Neural signals were recorded with a micro1401 A/D converter unit using Spike2 software (CED). Multiunit activity (MUA) and local field potential (LFP) were extracted from the raw signal with band-pass (300–3,000 Hz), and low pass (<150 Hz) electronic filters, respectively (Krohn-Hite, Inc). The laser Doppler flowmetry (LDF) signals were recorded at 200 Hz temporal resolution simultaneously with the electrical signals (1). Because the interoptode distance for the LDF probe was ∼200 μm, the effective spatial resolution of LDF was a half-ellipsoid of ∼0.1-μL volume. We checked the significance of neural and flow responses to forepaw stimulation with t test ($P < 0.001$) and only those individual time courses were selected, which passed the test. Then, the individual time series were averaged across subjects to provide the MUA, LFP, and cerebral blood flow (CBF) responses.

Multimodal fMRI Experiments. All fMRI (n = 12) data were obtained on an 11.7-T horizontal-bore spectrometer using a ^{1}H surface coil (Ø = 1.4 cm) in conjunction with a ^{1}H volume-coil (Ø = 6 cm) with echo planar imaging (EPI) using gradient-echo contrast. The field of view matrix size was 64 × 64 with slice thickness of 2 mm. The voxel point-spread function was about 450 μm and the analyzed slice was collected at the Bregma level. Blood oxygenation level-dependent (BOLD) signal was acquired with repetition time (TR) of 1 s and echo time (TE) of 15 ms. Cerebral blood volume (CBV) was recorded by the same EPI parameters, but CBV was recorded after an i.v. injection of iron-oxide nanocolloid particles (Combidex; 15 mg/kg; AMAG). For CBV, the nanoparticle has a several-hour half-life in blood circulation of rats (2). The BOLD effect was removed from the CBV-weighted signal (3, 4). In the presence of the MRI contrast agent the stimulation-induced decrease in the EPI signal reflected an increase in volume; therefore, all CBV-weighted fMRI data were multiplied by −1 to reflect positive changes in CBV during functional hyperemia. CBF was recorded without any contrast agents using arterial spin labeling (5). For CBF the detected slice was identical to those for BOLD and CBV, but an inversion pulse was used (with recovery delay of 2,100 ms) for flow tagging, by using alternating global inversion (no slice) or local inversion (slice thickness 10 mm) with a TR of 10 s, where the intensity difference in these images reflected the change in CBF (5). The averaged laminar LDF signals were scaled to the magnitude of the MRI-measured laminar CBF as previously described (3) so that the higher time resolution of the LDF signal was used for all time-domain analysis. All fMRI data were checked for translational movement criterion using a center-of-mass analysis (6). Those data that failed the test were discarded from further analysis. Single-run data were used to identify activation foci during stimulation and time courses were selected as the average of laminar activated voxels. Activation foci for fractional change in fMRI maps were obtained by applying Student t test between prestimulation and stimulation data. Three layers of the cortex were selected from the surface to the white matter using approximately equal spatial separation. Individual time courses of selected laminar activated voxels were averaged across many subjects. Statistical comparisons between parameters were conducted with one-way ANOVA.

Cerebral Metabolic Rate of Oxygen Consumption Calculations. Cerebral metabolic rate of oxygen consumption (CMR_{O2}) responses were calculated with calibrated fMRI using averaged BOLD, CBV, and CBF signals (7):

$$\frac{\Delta CMR_{O2}}{CMR_{O2}} = \frac{\Delta CBF}{CBF} - \left(\frac{1}{M}\frac{\Delta S}{S} + \frac{\Delta CBV}{CBV}\right)\left(1 + \frac{\Delta CBF}{CBF}\right),$$

where S is the BOLD signal and M is given by the product between TE and R_2' which is given by the absolute difference between the transverse relaxation rates with gradient echo (R_2^*) and spin echo (R_2) (i.e., $R_2' = R_2^* - R_2$). M was estimated to be 0.4 across all layers (Fig. S1), but for comparison we also calculated CMR_{O2} changes with M values of 0.3 and 0.5. The SD of the CMR_{O2} signal was calculated as error propagation of SDs of BOLD, CBV, and CBF signals. Because these modalities are not independent from each other we applied the Monte-Carlo method to calculate the error propagation of the CMR_{O2} SD (8).

Transfer Function Analysis. Convolution theory states that the input signal, I(t), when convolved with a transfer function, h(t), produces an output signal, O(t). In the case of neurovascular or neurometabolic coupling the input signal is the neural activity, either the LFP or the MUA, and the output signals are the CBF, CBV, BOLD, and CMR_{O2}. The specific transfer functions, h(t), can be achieved by deconvolution between O(t) and I(t). However, deconvolution does not provide an algorithmic solution for transfer function (9, 10); therefore, we used the gamma variate function as a model. We used a different form of the original equation so that the fitting parameters were independent from each other (11). We used a least-square mean Gauss–Newton fitting method with three steps as previously described (9, 10). The transfer functions were created for BOLD, CBF, and CBV

signals for three different layers as described above. However, the CMR_{O2} transfer functions were calculated with Eq. **1**, substituting the real responses with the transfer functions.

Correlations of Signals and Transfer Functions Between Layers. We selected only the evoked portions of our recorded time courses (or the whole transfer functions), normalized them to the middle layer response, and plotted the two signals originating from the two layers against each other. The pairs were upper vs. middle, upper vs. lower, and middle vs. lower. A linear regression line was fitted to the plot. The slope of the linear regression line and the Pearson correlation power (R^2) were calculated in every case. If the grade was close to 1 (line of identity), then we could consider the two signals to be identical.

Predicted Neural Signals. The advantage of the transfer function calculation is that the predicted signals (either calculated from the hemodynamic signals or from the CMR_{O2} signal) can be directly compared with the measured signals. Because the input signal cannot be modeled by an algorithmic function, a real deconvolution was necessary. Here we applied the Wiener deconvolution algorithm, following the description given by Glover (12) for its application to hemodynamic signal analysis. Using this method we could calculate the predicted neural signals from CMR_{O2} or any hemodynamic signals (BOLD, CBV, or CBF). If the transfer function (the mathematical definition of neurovascular and neuromatabolic couplings) is stable across all of the three studied layers, then the averaged transfer function (spanning across all layers) could reliably predict the neural activity for all of the layers. We compared the root mean-square value of the residue (residue = measured − predicted signals) for every layer and every modality to reveal which neural activity was best predicted.

1. Sanganahalli BG, Bailey CJ, Herman P, Hyder F (2009) Tactile and non-tactile sensory paradigms for fMRI and neurophysiologic studies in rodents. *Methods Mol Biol* 489: 213–242.
2. Kida I, Kennan RP, Rothman DL, Behar KL, Hyder F (2000) High-resolution CMR(O2) mapping in rat cortex: A multiparametric approach to calibration of BOLD image contrast at 7 Tesla. *J Cereb Blood Flow Metab* 20(5):847–860.
3. Kida I, Maciejewski PK, Hyder F (2004) Dynamic imaging of perfusion and oxygenation by functional magnetic resonance imaging. *J Cereb Blood Flow Metab* 24(12):1369–1381.
4. Lu H, Scholl CA, Zuo Y, Stein EA, Yang Y (2007) Quantifying the blood oxygenation level dependent effect in cerebral blood volume-weighted functional MRI at 9.4T. *Magn Reson Med* 58(3):616–621.
5. Kim SG (1995) Quantification of relative cerebral blood flow change by flow-sensitive alternating inversion recovery (FAIR) technique: Application to functional mapping. *Magn Reson Med* 34(3):293–301.
6. Chahboune H, et al. (2007) Neurodevelopment of C57B/L6 mouse brain assessed by in vivo diffusion tensor imaging. *NMR Biomed* 20(3):375–382.
7. Hyder F, et al. (2001) Quantitative functional imaging of the brain: Towards mapping neuronal activity by BOLD fMRI. *NMR Biomed* 14(7-8):413–431.
8. Ogilvie JF (1984) A Monte-Carlo approach to error propagation. *Comput Chem* 8(3): 205–207.
9. Herman P, Sanganahalli BG, Blumenfeld H, Hyder F (2009) Cerebral oxygen demand for short-lived and steady-state events. *J Neurochem* 109(Suppl 1):73–79.
10. Sanganahalli BG, Herman P, Blumenfeld H, Hyder F (2009) Oxidative neuroenergetics in event-related paradigms. *J Neurosci* 29(6):1707–1718.
11. Madsen M (1992) A simplified formulation of the gamma variate function. *Phys Med Biol* 37:1597–1600.
12. Glover GH (1999) Deconvolution of impulse response in event-related BOLD fMRI. *Neuroimage* 9(4):416–429.

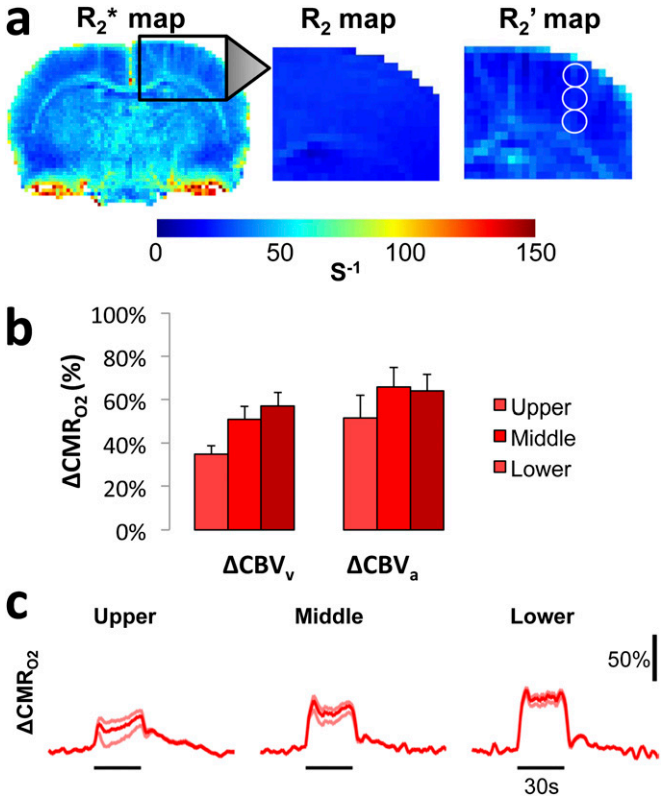

Fig. S1. Parameters affecting calculating changes in cerebral metabolic rate of oxygen consumption (CMR_{O2}) from the blood oxygenation level-dependent (BOLD) signal. (*A*) Transverse relaxation rate maps of a representative rat brain at rest. Under good shim conditions, transverse relaxation rates of gradient echo (R_2*, *Left*) and spin-echo (R_2, *Center*) were acquired with several echo time (TE) values. Difference between R_2* and R_2 (i.e., R_2*− R_2) reveals the most sensitive BOLD component (R_2', *Right*), where the product between R_2' and TE gives the *M* parameter in Eq. **1**. The circles in the R_2' map represent the three selected laminar regions of the forepaw area. The average cortical R_2' value was 25 ± 3 s^{-1}, which is equivalent to $M = 0.4 \pm 0.04$ with a TE of 15 ms. (*B*) The impact of the cerebral blood volume (CBV) term in Eq. **1** for calculating changes in CMR_{O2} depends on which vascular compartment the changes occur. Because current assumptions about BOLD signal is that the oxygenation and volume changes primarily occur at the venous end, the CBV term in Eq. **1** is thought to represent predominantly the venous compartment (ΔCBV_v). The current calculations of changes in CMR_{O2} in Fig. 1*D* were made with ΔCBV_v as represented by the measured laminar CBV changes shown in Fig. 1*B*. If, however, the measured laminar CBV changes occurred primarily in the arterial compartment (ΔCBV_a), then the contribution of the CBV term in Eq. **1** would be completely removed. The impacts of these two CBV assumptions on changes in CMR_{O2} with Eq. **1** are respectively shown on the left and right, where similar laminar trends are noted. (*C*) The impact of 25% (±0.1) change in *M* value (light red traces) for the calculated CMR_{O2} time series (red traces) shown in Fig. 1*D*.

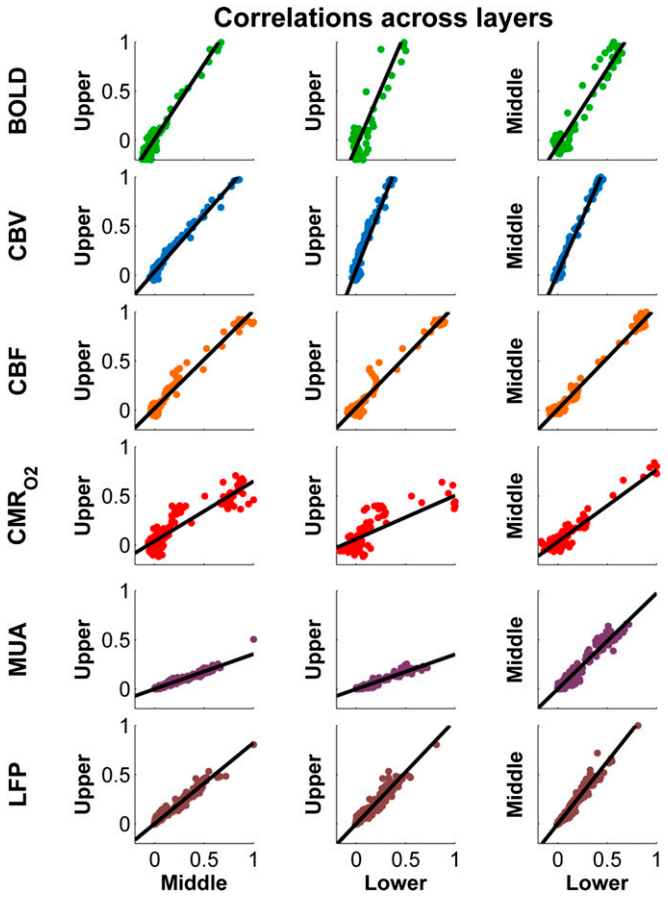

Fig. S2. Correlations of stimulation-induced responses across cortical lamina. All of the responses were normalized to the responses of the middle layer. Then, the normalized functional responses from upper, middle, and lower layers were plotted against each other plotting the respective data points of response time course from one layer vs. another layer. The linear regression line is shown in black, whereas the data points are shown by the dots. The respective values of slope and Pearson correlation power (r^2) are listed in Table S2.

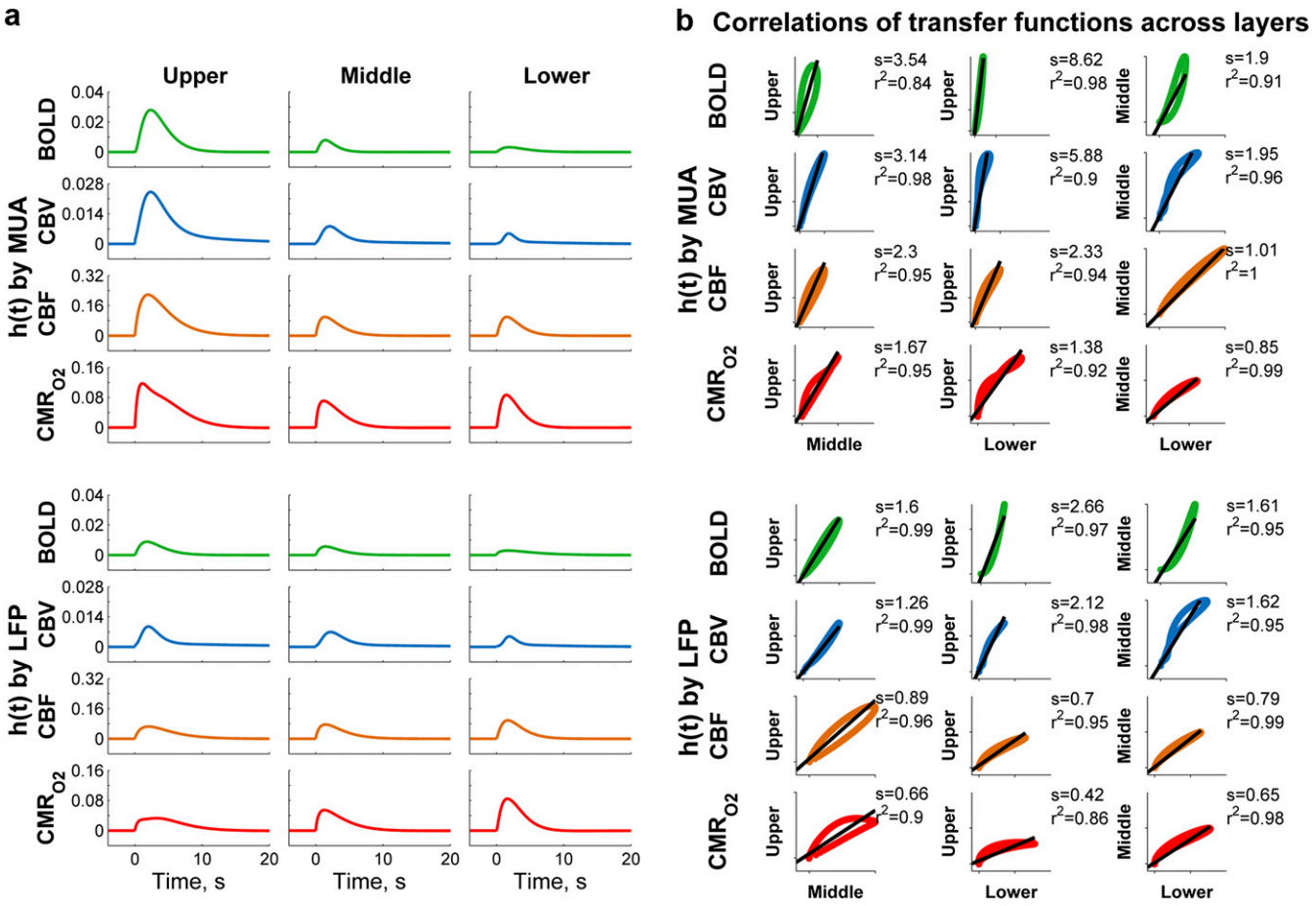

Fig. S3. Correlations of transfer functions across cortical lamina. The transfer functions from all layers, for each modality (i.e., h_x), were compared without normalization. (*A*) Comparison of layer-specific transfer function for each modality, where either MUA (*Upper*) or LFP (*Lower*) was used as the input in the convolution analysis (*SI Materials and Methods*). (*B*) A linear regression analysis was performed, for each modality, by comparing the transfer function of one layer vs. another layer, where either MUA (*Upper*) or LFP (*Lower*) was used as the input in the convolution analysis (*SI Materials and Methods*). The respective slope values of the regression line and the Pearson correlation power (r^2) of the linear regression are shown in Table S3.

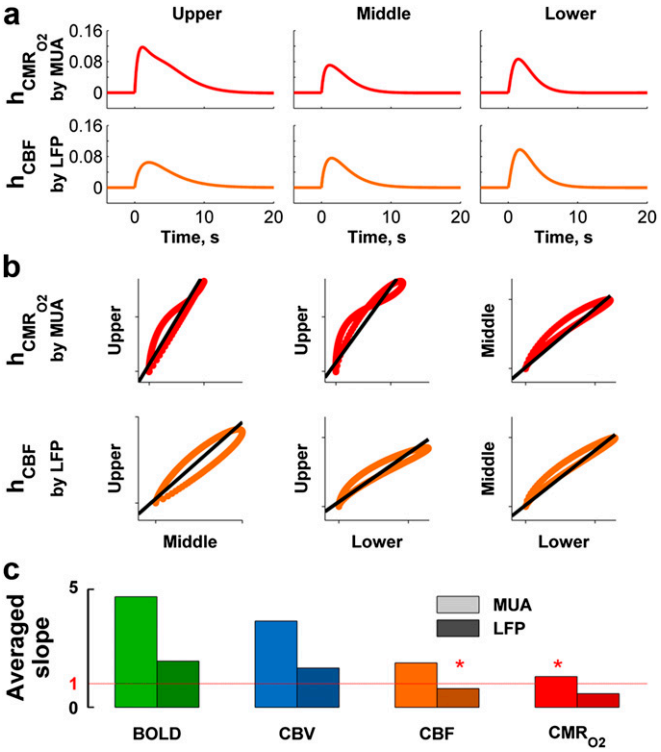

Fig. S4. Transfer functions were used to provide a mathematical connection between input and output signals of a system. Transfer function for each modality was derived from the neural input. Convolution analysis (*SI Materials and Methods*) was used to find a transfer function that connects the neural response (input) to either hemodynamic or metabolic response (output) and gives the mathematical definition of neurovascular/metabolic coupling. (*A*) Layer-specific transfer functions of CMR_{O2} (h_{CMRO2}) and CBF (h_{CBF}) were calculated with MUA and LFP, respectively, as the inputs. The layer-specific h_{CBF} were quite uniform, whereas only the h_{CMRO2} in middle and lower segments were comparable. (*B*) Correlation of transfer functions across different layers for CMR_{O2} (*Top*) and CBF (*Bottom*). The layer-specific h_{CBF} were quite interchangeable, whereas only the h_{CMRO2} located in middle and lower segments were interchangeable. Table S3 and Fig. S3 give details on correlations of all other multimodal transfer responses across layers. (*C*) For each modality, a linear regression analysis was performed by plotting the transfer function, with MUA (lighter shade) and LFP (darker shade) as input, of one layer vs. another layer as described above for h_{CMRO2} (Fig. S3*A*) and h_{CBF} (Fig. S3*B*), where for a given modality the average slope of the regressions from all three permutations of layer comparisons (i.e., upper vs. middle, upper vs. lower, and middle vs. lower) if close to 1 indicates higher predictive power of the respective transfer function. The averaged h_{CMRO2} and h_{CBF} performed better than all other transfer functions to predict MUA and LFP, respectively (indicated by *). The asterisks on the left CBF column and the right CMR_{O2} column, respectively, suggest that the CBF transfer function derived from LFP (h_{CBF}) and the CMR_{O2} transfer function derived from MUA (h_{CMRO2}) have the highest predictive powers to calculate LFP and MUA, respectively, with measured CBF and CMR_{O2} (Fig. 3).

Table S1. Time constants for rise and decay of responses across cortical lamina measured with MRI methods

	BOLD		CBV		CBF		CMR_{O2}	
Cortical lamina	Rise	Decay	Rise	Decay	Rise	Decay	Rise	Decay
Upper	3.3 ± 0.2 (r^2 = 0.94)	4.3 ± 0.6 (r^2 = 0.82)	3.0 ± 0.3 (r^2 = 0.92)	14.2 ± 0.2 (r^2 = 0.99)	2.2 ± 0.3 (r^2 = 0.93)	8.7 ± 0.3 (r^2 = 0.97)	2.6 ± 0.3 (r^2 = 0.92)	11.0 ± 0.8 (r^2 = 0.86)
Middle	3.4 ± 0.2 (r^2 = 0.94)	4.1 ± 0.4 (r^2 = 0.89)	3.1 ± 0.2 (r^2 = 0.94)	10.5 ± 0.2 (r^2 = 0.99)	2.1 ± 0.3 (r^2 = 0.94)	6.4 ± 0.5 (r^2 = 0.91)	2.3 ± 0.3 (r^2 = 0.93)	9.2 ± 0.7 (r^2 = 0.86)
Lower	3.6 ± 0.2 (r^2 = 0.91)	7.5 ± 0.4 (r^2 = 0.96)	3.2 ± 0.2 (r^2 = 0.95)	8.1 ± 0.3 (r^2 = 0.97)	2.3 ± 0.3 (r^2 = 0.92)	6.0 ± 0.7 (r^2 = 0.79)	2.8 ± 0.3 (r^2 = 0.93)	6.5 ± 0.8 (r^2 = 0.71)

Each time constant is shown as mean ± SD (units in seconds), calculated by a single exponential fit where r^2 reflects the goodness of the fit to the data. The time constant represents the time the response takes to reach two-thirds of the peak value, both following stimulation onset (i.e., rise) and offset (i.e., decay). There were no significant differences in response rise times across cortical lamina for any modality (one-way ANOVA). However, response decay times across cortical lamina of specific modalities were significantly different ($P < 0.01$; one-way ANOVA). For BOLD decay only the middle vs. lower was significant. For CBV decay upper vs. middle, upper vs. lower, and middle vs. lower were significant. For CBF decay none of the comparisons was significant. For CMR_{O2} decay only the upper vs. middle was insignificant. The slowest and fastest time-to-peak values were, respectively, observed for BOLD (transcortical range of 3.3–3.6 s) and CBF (transcortical range of 2.1–2.3 s) laminar responses, whereas the time-to-peak values of layer-specific responses of CBV and CMR_{O2} were intermediate (transcortical ranges of 3.0–3.2 s and 2.3–2.8 s, respectively). The BOLD decay times in middle and lower segments were significantly different (i.e., 4.1 s vs. 7.5 s with one-way ANOVA), and moreover the BOLD responses from upper and middle laminae showed small poststimulation dips (Fig. 1*A*). The CBV decay times in upper, middle, and lower laminae were significantly different from each other (transcortical range of 8.1–14.2 s; Fig. 1*B*). The laminar CBF decay times were not distinctly different from each other (transcortical range of 6.0–8.7 s; Fig. 1*C*), whereas the CMR_{O2} decay times in upper and middle segments were insignificantly different (transcortical range of 6.5–11.0 s; Fig. 1*D*).

Table S2. Correlations of functional responses across cortical lamina

Regression analysis	BOLD	CBV	CBF	CMR_{O2}	MUA	LFP
Upper vs. middle	$1.5 \pm 1.3 \cdot 10^{-10}$ ($r^2 = 0.99$)	$1.2^{\dagger} \pm 8.4 \cdot 10^{-9}$ ($r^2 = 1.00$)	$1.0^{\dagger} \pm 2.3 \cdot 10^{-11}$ ($r^2 = 0.99$)	$0.5 \pm 3.4 \cdot 10^{-11}$ ($r^2 = 0.91$)	$0.4 \pm 1.7 \cdot 10^{-11}$ ($r^2 = 0.98$)	$0.8^{\dagger} \pm 2.4 \cdot 10^{-11}$ ($r^2 = 0.99$)
Upper vs. lower	$2.3 \pm 1.4 \cdot 10^{-10}$ ($r^2 = 0.96$)	$2.6 \pm 1.5 \cdot 10^{-10}$ ($r^2 = 0.99$)	$1.0^{\dagger} \pm 6.9 \cdot 10^{-11}$ ($r^2 = 0.99$	$0.4 \pm 3.4 \cdot 10^{-11}$ ($r^2 = 0.88$)	$0.4 \pm 2.4 \cdot 10^{-11}$ ($r^2 = 0.98$)	$1.0^{\dagger} \pm 2.4 \cdot 10^{-11}$ ($r^2 = 0.98$)
Middle vs. lower	$1.6 \pm 1.1 \cdot 10^{-10}$ ($r^2 = 0.97$)	$2.3 \pm 1.6 \cdot 10^{-10}$ ($r^2 = 0.99$)	$1.0^{\dagger} \pm 6.9 \cdot 10^{-11}$ ($r^2 = 0.99$)	$0.8^{\dagger} \pm 6.1 \cdot 10^{-11}$ ($r^2 = 0.98$)	$1.0^{\dagger} \pm 2.1 \cdot 10^{-11}$ ($r^2 = 0.98$)	$1.2^{\dagger} \pm 8.9 \cdot 10^{-11}$ ($r^2 = 0.99$)

The functional responses from all layers, for each modality, were normalized to the response from the middle layer. For each modality, a linear regression analysis was performed by comparing the normalized functional responses of one layer vs. another layer (Fig. S2). The slope values of the regression line are shown without parentheses, whereas the values within the parentheses represent the Pearson correlation power (r^2) of the linear regression. If the slope is close to 1, then the compared responses are similar (indicated by †). The SDs of the slope values were calculated with Monte-Carlo simulation from 40,000 realizations each. Figs. 1 and 2 show details on correlations of functional responses.

Table S3. Correlations of transfer functions across cortical lamina

Regression analysis	h_{BOLD}		h_{CBV}		h_{CBF}		h_{CMRO2}	
	By MUA	By LFP	By MUA	By LFP	By MUA	By LFP	By MUA	By LFP
Upper vs. middle	3.5 ($r^2 = 0.84$)	1.6 ($r^2 = 0.99$)	3.1 ($r^2 = 0.98$)	1.3 ($r^2 = 0.99$)	2.3 ($r^2 = 0.95$)	$0.9^{\dagger}$ ($r^2 = 0.96$)	1.7 ($r^2 = 0.95$)	0.7 ($r^2 = 0.90$)
Upper vs. lower	8.6 ($r^2 = 0.98$)	2.7 ($r^2 = 0.97$)	5.9 ($r^2 = 0.90$)	2.1 ($r^2 = 0.98$)	2.3 ($r^2 = 0.94$)	$0.7^{\dagger}$ ($r^2 = 0.95$)	1.4 ($r^2 = 0.92$)	0.4 ($r^2 = 0.86$)
Middle vs. lower	1.9 ($r^2 = 0.91$)	1.6 ($r^2 = 0.95$)	2.0 ($r^2 = 0.96$)	1.6 ($r^2 = 0.95$)	$1.0^{\dagger}$ ($r^2 = 1.00$)	$0.8^{\dagger}$ ($r^2 = 0.99$)	$0.9^{\dagger}$ ($r^2 = 0.99$)	0.7 ($r^2 = 0.98$)
Average	4.7 ± 3.5	2.0 ± 0.6	3.7 ± 2.0	1.7 ± 0.3	1.9 ± 0.8	$0.8 \pm 0.1^{\dagger}$	$1.3 \pm 0.4^{\dagger}$	0.6 ± 0.1

The transfer functions from all layers, for each modality (i.e., h_x), were compared without normalization. For each modality, a convolution analysis (*SI Materials and Methods*) was performed to generate the transfer function per layer, where either MUA or LFP was used as the input (Fig. S3*A*). For each modality, a linear regression analysis was then performed by comparing the transfer function of one layer vs. another layer (Fig. S3*B*). The slope values of the regression line are shown without parentheses, whereas the values within the parentheses represent the Pearson correlation power (r^2) of the linear regression. If the slope is close to 1, then the compared transfer functions are similar (indicated by †). The Average row represents the mean of layer-specific values. Fig. S4 shows a summary of correlations for transfer functions for each modality.

Table S4. Predictive power of neural responses across cortical lamina

Residual analysis	Upper, R_x				Middle, R_x				Lower, R_x				Overall, ΣR_x			
	BOLD	CBV	CBF	CMR_{O2}	BOLD	CBV	CBF	CMR_{O2}	BOLD	CBV	CBF	CMR_{O2}	BOLD	CBV	CBF	CMR_{O2}
MUA	0.82	0.47	0.25	0.04	0.01	0.01	0.00	0.01	0.04	0.13	0.01	0.05	0.87	0.61	0.26	$0.10^{\dagger}$
LFP	0.28	0.07	0.02	0.04	0.02	0.04	0.01	0.01	0.01	0.06	0.04	0.11	0.31	0.17	$0.07^{\dagger}$	0.16

The predictive power of neural responses from the transfer function per layer for a given modality (Fig. S3*A*) was based on a residual analysis. The Wiener deconvolution algorithm was applied to predict the neural response (*SI Materials and Methods*). For a given modality x, a residual value (R_x) was calculated using the root mean square of the difference between predicted and measured responses for the entire functional data set. The sum of R_x values across all cortical layers (ΣR_x) was used to reflect the predictive power of neural responses. Higher predictive power was suggested if ΣR_x was close to 0 (indicated by † in the Overall columns).